Acta Cryst E CRYSTALLOGRAPHIC COMMUNICATIONS

ISSN 2056-9890

N,*N*′-Bis(pyridin-3-ylmethyl)ethanediamide monohydrate: crystal structure, Hirshfeld surface analysis and computational study

Sang Loon Tan and Edward R. T. Tiekink*

Research Centre for Crystalline Materials, School of Science and Technology, Sunway University, 47500 Bandar Sunway, Selangor Darul Ehsan, Malaysia. *Correspondence e-mail: edwardt@sunway.edu.my

Received 28 November 2019
Accepted 2 December 2019

Edited by W. T. A. Harrison, University of Aberdeen, Scotland

Keywords: crystal structure; diamide; hydrogen bonding; Hirshfeld surface analysis; computational chemistry.

CCDC reference: 1969282

Supporting information: this article has supporting information at journals.iucr.org/e

The molecular structure of the title bis-pyridyl substituted diamide hydrate, $C_{14}H_{14}N_4O_2{\cdot}H_2O$, features a central $C_2N_2O_2$ residue (r.m.s. deviation = 0.0205 Å) linked at each end to 3-pyridyl rings through methylene groups. The pyridyl rings lie to the same side of the plane, *i.e.* have a *syn*-periplanar relationship, and form dihedral angles of 59.71 (6) and 68.42 (6)° with the central plane. An almost orthogonal relationship between the pyridyl rings is indicated by the dihedral angle between them [87.86 (5)°]. Owing to an *anti* disposition between the carbonyl-O atoms in the core, two intramolecular amide-N—H···O(carbonyl) hydrogen bonds are formed, each closing an *S*(5) loop. Supramolecular tapes are formed in the crystal *via* amide-N—H···O(carbonyl) hydrogen bonds and ten-membered $\{\cdots HNC_2O\}_2$ synthons. Two symmetry-related tapes are linked by a helical chain of hydrogen-bonded water molecules *via* water-O—H···N(pyridyl) hydrogen bonds. The resulting aggregate is parallel to the *b*-axis direction. Links between these, *via* methylene-C—H···O(water) and methylene-C—H···π(pyridyl) interactions, give rise to a layer parallel to $(10\bar{1})$; the layers stack without directional interactions between them. The analysis of the Hirshfeld surfaces point to the importance of the specified hydrogen-bonding interactions, and to the significant influence of the water molecule of crystallization upon the molecular packing. The analysis also indicates the contribution of methylene-C—H···O(carbonyl) and pyridyl-C—H···C(carbonyl) contacts to the stability of the inter-layer region. The calculated interaction energies are consistent with importance of significant electrostatic attractions in the crystal.

1. Chemical context

Having both amide and pyridyl functionality, bis(pyridin-*n*-ylmethyl)ethanediamide molecules of the general formula *n*-$NC_5H_4CH_2N(H)C(=O)C(=O)CH_2C_5H_4N$-*n*, for *n* = 2, 3 and 4, hereafter $^nLH_2$, are attractive co-crystal coformers *via* conventional hydrogen bonding. In the same way, complexation to metals may also be envisaged. It is therefore not surprising that there is now a wealth of structural information for these molecules occurring in co-crystals, salts and metal complexes, as has been reviewed recently (Tiekink, 2017). Complementing hydrogen-bonding interactions, the $^nLH_2$ molecules, for *n* = 3 (Hursthouse *et al.*, 2003; Goroff *et al.*, 2005; Jin *et al.*, 2013) and *n* = 4 (Goroff *et al.*, 2005; Wilhelm *et al.*, 2008; Tan & Tiekink, 2019*c*), are well-known to form N···I halogen-bonding interactions and, indeed, some of the earliest studies were at the forefront of pioneering systematic investigations of halogen bonding. It was during the course of ongoing studies into co-crystal formation (Tan, Halcovitch *et al.*,

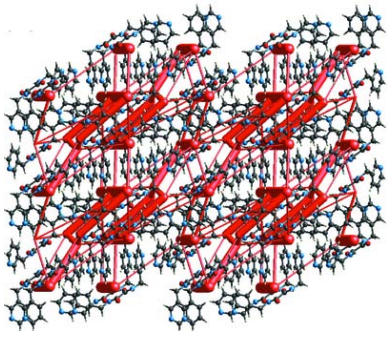

2019; Tan & Tiekink, 2019*a*,*b*,*c*) and complexation to zinc(II) 1,1-dithiolates (Arman *et al.*, 2018; Tiekink, 2018; Tan, Chun *et al.*, 2019), that the title compound, $^3LH_2{\cdot}H_2O$, (I), was isolated. Herein, the crystal and molecular structures of (I) are described along with a detailed analysis of the molecular packing by means of an analysis of the calculated Hirshfeld surfaces, two-dimensional fingerprint plots and the calculation of energies of interaction.

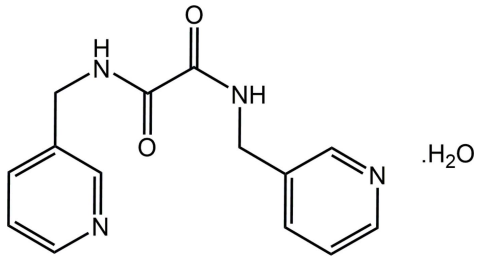

2. Structural commentary

The molecular structures of the two constituents comprising the crystallographic asymmetric unit of (I) are shown in Fig. 1. The $^3LH_2$ molecule lacks crystallographic symmetry and comprises a central $C_2N_2O_2$ residue connected at either side to two 3-pyridyl residues *via* methylene links. The six atoms of the central residue are almost co-planar as seen in their r.m.s. deviation of 0.0205 Å: the maximum deviations above and below the plane are 0.0291 (9) Å for N3 and 0.0321 (11) Å for C8. The N1- and N3-pyridyl rings form dihedral angles of 59.71 (6) and 68.42 (6)°, respectively, with the central plane and lie to the same side of the plane, having a *syn*-periplanar relationship. The dihedral angle formed between the pyridyl rings is 87.86 (5)°, indicating an almost edge-to-face relationship. The carbonyl-O atoms have an *anti* disposition enabling the formation of intramolecular amide-N—H···O(carbonyl) hydrogen bonds that close *S*(5) loops, Table 1.

3. Supramolecular features

Significant conventional hydrogen bonding is noted in the crystal of (I) with the geometric parameters characterizing these included in Table 1. The most striking feature of the supramolecular association is the formation of tapes *via* amide-N—H···O(carbonyl) hydrogen bonds leading to a sequence of inter-connected ten-membered $\{\cdots HNC_2O\}_2$ synthons. Two such tapes are connected by hydrogen bonds provided by the water molecule of crystallization. Thus, alternating water molecules in helical chains of hydrogen-bonded water molecules, being aligned along the *b*-axis direction and propagated by 2_1 symmetry, connect to $^3LH_2$ *via* water-O—H···N(pyridyl) hydrogen bonds to form the one-dimensional aggregate shown in Fig. 2(*a*). The presence of methylene-C—H···O(water) and methylene-C—H···π(pyridyl) contacts stabilizes a layer lying parallel to $(10\overline{1})$. The layers stack without directional interactions between them, Fig. 2(*b*).

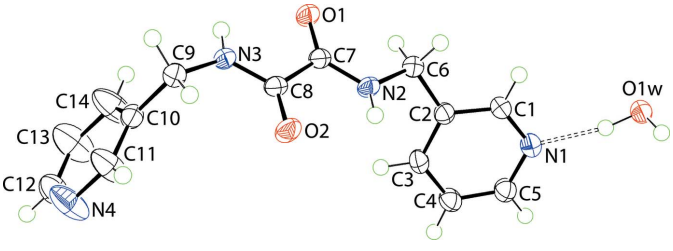

Figure 1
The molecular structure of the constituents of (I) showing the atom-labelling scheme and displacement ellipsoids at the 70% probability level. The water-O—H···N(pyridyl) hydrogen bond is indicated by the dashed line.

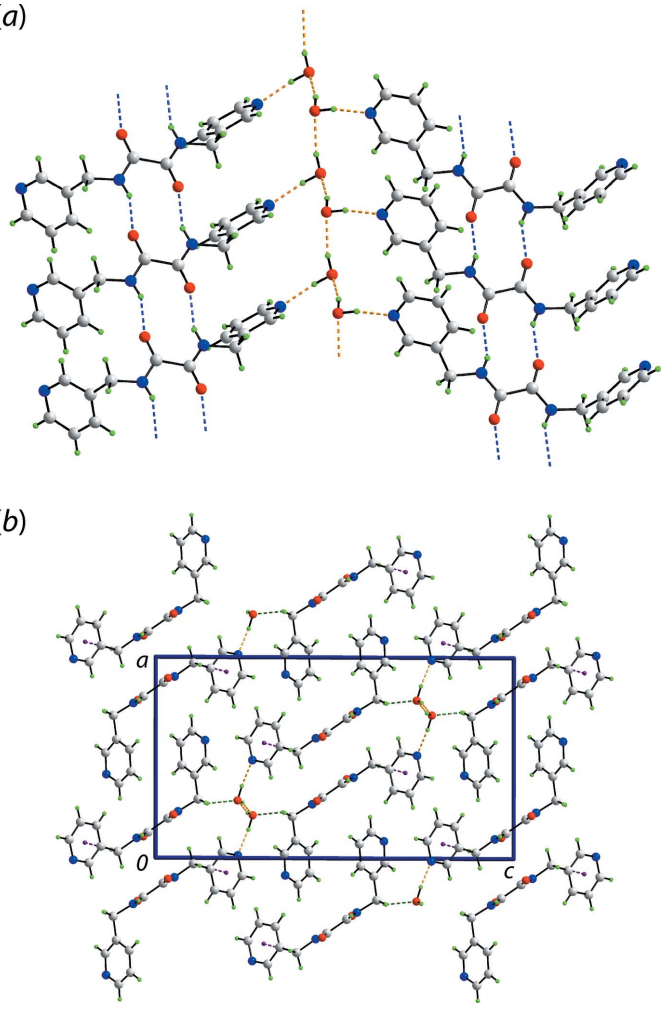

Figure 2
Molecular packing in the crystal of (I): (*a*) one-dimensional chain whereby tapes sustained by amide-N—H···O(carbonyl) hydrogen bonds and ten-membered $\{\cdots HNC_2O\}_2$ synthons are connected, *via* water-O—H···N(pyridyl) hydrogen bonds, by helical chains of hydrogen-bonded water molecules sustained by water-O—H···O(water) hydrogen bonds and (*b*) a view of the unit-cell contents in projection down the *b* axis, highlighting the stacking of layers. The amide-N—H···O(carbonyl) hydrogen bonds are shown as blue dashed lines and hydrogen bonds involving the water molecules, by orange dashed lines. The C—H···O and C—H···π interactions are shown as green and purple dashed lines, respectively.

Table 1
Hydrogen-bond geometry (Å, °).

D—H···A	D—H	H···A	D···A	D—H···A
N2—H2N···O2	0.85 (2)	2.36 (2)	2.7279 (18)	107.0 (16)
N3—H3N···O1	0.86 (2)	2.299 (19)	2.6924 (18)	108.0 (15)
O1W—H1W···N1	0.95 (2)	1.86 (2)	2.7958 (18)	169 (2)
O1W—H2W···O1W^{i}	0.88 (2)	1.97 (2)	2.8364 (15)	166 (2)
N2—H2N···O1^{ii}	0.85 (2)	2.03 (2)	2.8227 (18)	155.2 (18)
N3—H3N···O2^{iii}	0.86 (2)	2.02 (2)	2.8022 (18)	151.6 (17)
C9—H9A···O1W^{iv}	0.99	2.45	3.3772 (19)	156
C6—H6B···Cg1^{iii}	0.99	2.74	3.7043 (16)	166

Symmetry codes: (i) $-x+\frac{3}{2}, y+\frac{1}{2}, -z+\frac{3}{2}$; (ii) $x, y+1, z$; (iii) $x, y-1, z$; (iv) $x-\frac{1}{2}, -y+\frac{1}{2}, z-\frac{1}{2}$.

Table 2
Summary of short interatomic contacts (Å) in (I)[a].

Contact	Distance	Symmetry operation
O2···H3N	1.89	$x, 1+y, z$
O1···H2N	1.89	$x, -1+y, z$
O2···H6A	2.57	$1-x, 1-y, 1-z$
N4···H5	2.52	$-\frac{1}{2}+x, \frac{3}{2}-y, -\frac{1}{2}+z$
C7···H12	2.64	$-x, -y, 1-z$
O1W···H1	2.55	$\frac{3}{2}-x, \frac{1}{2}+y, \frac{3}{2}-z$
C7···O1	3.16	$1-x, -y, 1-z$
N1···H1W	1.83	x, y, z

Notes: (*a*) The interatomic distances were calculated in *Crystal Explorer 17* (Turner *et al.*, 2017) whereby the X—H bond lengths are adjusted to their neutron values.

4. Hirshfeld surface analysis

The calculations of the Hirshfeld surfaces and two-dimensional fingerprint plots were performed on the crystallographic asymmetric unit shown in Fig. 1, using *Crystal Explorer 17* (Turner *et al.*, 2017) and based on the procedures as described previously (Tan, Jotani *et al.*, 2019). The analysis identified a number of red spots on the $d_{\rm norm}$ surface of $^{3}LH_2$ with varying degrees of intensity indicating the presence of interactions with contact distances shorter than the sum of the respective van der Waals radii (Spackman & Jayatilaka, 2009). Referring to the images of Fig. 3, the most intense red spots stem from the amide-N—H···O(carbonyl) and water-O—H···N(pyridyl) hydrogen bonds, Table 1. Some additional contacts are detected through the Hirshfeld surface analysis for C1—H1···O1W, C5–H5···N4, C12—H12···C7, C6–H6A···O2 and C7···O1 interactions with the red spots ranging from moderately to weakly intense. The data in Table 2 provide a succinct summary of interatomic contacts revealed in the above analysis; the O2···H6A and C7···H12 contacts occur in the inter-layer region.

To verify the nature of the aforementioned interactions, the $^{3}LH_2$ molecule in (I) was subjected to electrostatic potential mapping. The results show that almost all of the interactions identified through the $d_{\rm norm}$ mapping are electrostatic in nature as can be seen from the distinctive blue (electro-

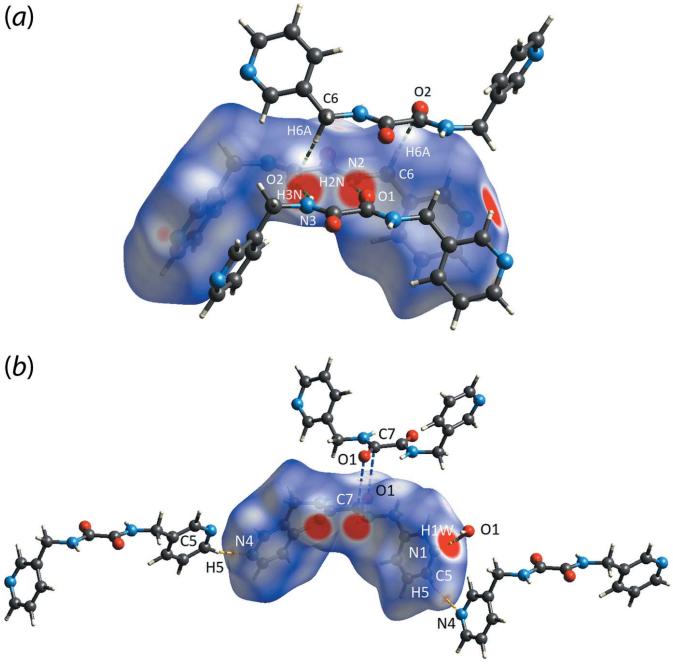

Figure 3
The $d_{\rm norm}$ mapping of the Hirshfeld surface for $^{3}LH_2$ in (I) within the range of −0.3259 to 1.0656 arbitrary units, showing the red spots for (*a*) N2—H2N···O1 (intense, connected by green dashed line), N3—H3N···O2 (intense, green dashed line) and C6—H6A···O2 (diminutive, green dashed line) interactions, (*b*) O1W—H1W···N1 (intense, yellow dashed line), C5—H5···N4 (moderately intense, yellow dashed line) and C7···O1 (diminutive, blue dashed line) interactions.

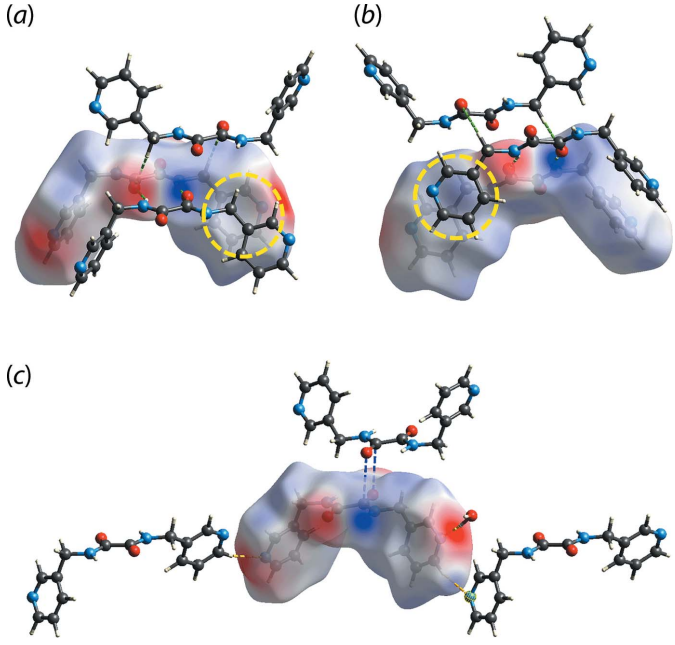

Figure 4
The electrostatic potential mapped onto the Hirshfeld surface within the isosurface value of −0.0964 to 0.1012 atomic units for $^{3}LH_2$ in (I), showing the charge complementarity for (*a*) C6—H6A···O2 (green dashed lines), (*b*) N2—H2N···O1 and N3—H3N···O2 (green dashed lines) and (*c*) C5—H5···N4 (yellow dashed line), O1W—H1W···N1 (yellow dashed line) and C7···O1 (blue dashed lines) interactions. The yellow circles in (*a*) and (*b*) highlight the dispersive nature of the methylene-C—H···π(pyridyl) interaction with no charge complementarity.

positive) and red (electronegative) regions on the surface, albeit with varying intensity, Fig. 4. A notable exception is found for the methylene-C—H···π(pyridyl) interaction which is manifested in the pale regions in Fig. 4(*a*) and (*b*). This indicates no charge complementarity consistent with the interaction beings mainly dispersive in nature.

The quantification of the close contacts to the Hirshfeld surface was performed through the analysis of the two-dimensional fingerprint plots for (I) as well as for the individual molecular components. As shown in Fig. 5(*a*), the overall fingerprint plot of (I) exhibits a bug-like profile with a pair of symmetric spikes. This is in contrast to the asymmetric profile of $^3LH_2$, with splitting of the spike in the internal region due to the formation of the O—H···N hydrogen bond, Fig. 5(*e*), suggesting a prominent role played by the water molecule in influencing the overall contacts in (I). The observation is very

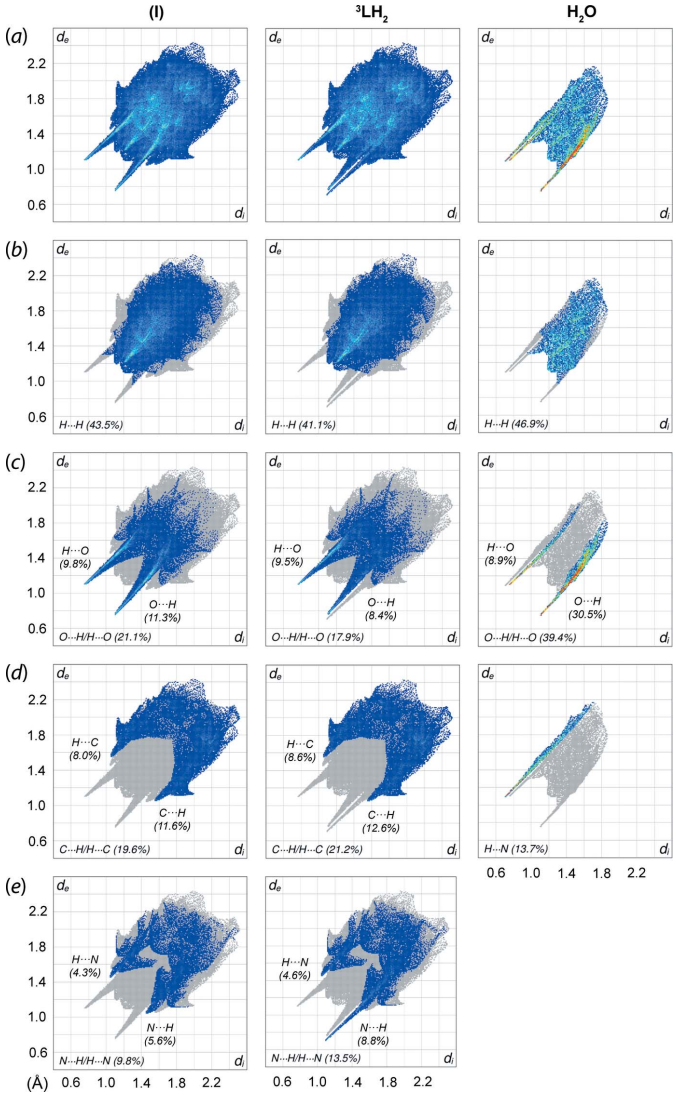

Figure 5
(*a*) The overall two-dimensional fingerprint plots for (I) and for the individual $^3LH_2$ and water molecules, and those delineated into (*b*) H···H, (*c*) H···O/O···H, (*d*) H···C/C···H and (*e*) H···N/N···H contacts. The percentage contributions to the surfaces are indicated therein.

Table 3
Summary of interaction energies (kJ mol^{-1}) calculated for (I).

Contact	E_{ele}	E_{pol}	E_{dis}	E_{rep}	E_{tot}
N2—H2*N*···O1^{i} +					
N3—H3*N*···O2^{i}	−68.5	−15.0	−49.2	86.4	−73.0
C12—H12···C7^{ii}	−6.7	−2.0	−46.1	26.0	−32.7
C6—H6*A*···O2^{iii}	−12.9	−2.9	−28.2	13.5	−32.0
O1*W*—H1*W*···N1^{iv}	−51.9	−11.2	−6.5	65.1	−28.6
O1*W*—H2*W*···O1*W*^{v}	−36.9	−7.1	−3.5	34.3	−26.2
C7···O1^{vi}	−2.3	−3.0	−31.4	18.4	−20.7
C5—H5···N4^{vii}	−9.4	−2.0	−8.1	8.7	−13.0
C1—H1···O1*W*^{viii}	−8.1	−1.3	−3.9	3.9	−10.5

Symmetry operations: (i) $x, 1+y, z$; (ii) $-x, -y, 1-z$; (iii) $1-x, 1-y, 1-z$; (iv) x, y, z; (v) $\frac{3}{2}-x, \frac{1}{2}+y, \frac{3}{2}-z$; (vi) $1-x, -y, 1-z$; (vii) $\frac{1}{2}+x, \frac{3}{2}-y, \frac{1}{2}+z$; (viii) $\frac{3}{2}-x, -\frac{1}{2}+y, \frac{3}{2}-z$.

different to that of the benzene solvate of $^4LH_2$ in which the overall surface contacts for $^4LH_2$ are not very much influenced by the benzene molecule as demonstrated by the similar profiles for the solvate and individual $^4LH_2$ molecule (Tan, Halcovitch *et al.*, 2019). The decomposition of the overall profile of (I) shows that the most significant contacts are primarily H···H contacts (43.5%), followed by O···H/H···O (21.1%), C···H/H···C (19.6%) and N···H/H···N (9.8%) contacts, with all of these interactions having $d_i + d_e$ distances less than the respective sums of van der Waals radii (vdW), *i.e.* H···H ∼2.26 Å [Σ(vdW) = 2.40 Å], O···H/H···O ∼1.88 Å [Σ(vdW) = 2.72 Å], C···H/H···C ∼2.62 Å [Σ(vdW) = 2.90 Å] and N···H/H···N ∼2.50 Å [Σ(vdW) = 2.75 Å].

As for the individual $^3LH_2$ molecule, the dominance of these contacts follows the order H···H (41.1%; $d_i + d_e$ 2.33 Å), C···H/H···C (21.2%; $d_i + d_e$ 2.60 Å), O···H/H···O (17.9%; $d_i + d_e$ 1.88 Å) and N···H/H···N (13.5%; $d_i + d_e$ 1.80 Å). While the aforementioned interactions are almost evenly distributed between the internal and external contacts for (I), some contacts for $^3LH_2$ are found to either to be inclined towards the internal or external contact region compared with (I), such as that displayed by (internal)-O···H-(external) (8.4%) *versus* (internal)-H···O-(external) (9.5%) and (internal)-N···H-(external) (8.8%) *versus* (internal)-H···N-(external) (4.6%), respectively, Fig. 5(*c*)–(*e*).

The hydrate molecule exhibits a completely different fingerprint profile, which is dominated by three major contacts, namely H···H (46.9%; $d_i + d_e$ 2.26 Å), O···H/H···O (39.4%; $d_i + d_e$ 1.88 Å) and H···N (13.7%; $d_i + d_e$ 1.80 Å). In particular, the second most dominant contacts are found to be heavily inclined toward (internal)-O···H-(external) (30.5%) as compared to (internal)-H···O-(external) (8.9%), presumably due to relatively large contact surface area.

5. Computational chemistry

All associations between molecules in (I), as described in *Hirshfeld surface analysis*, were subjected to the calculation of the interaction energy using *Crystal Explorer 17* (Turner *et al.*, 2017) based on the method described previously (Tan, Jotani *et al.*, 2019) to evaluate the strength of each interaction, Table 3. Among those close contacts, the $(^3LH_2)_2$ dimer

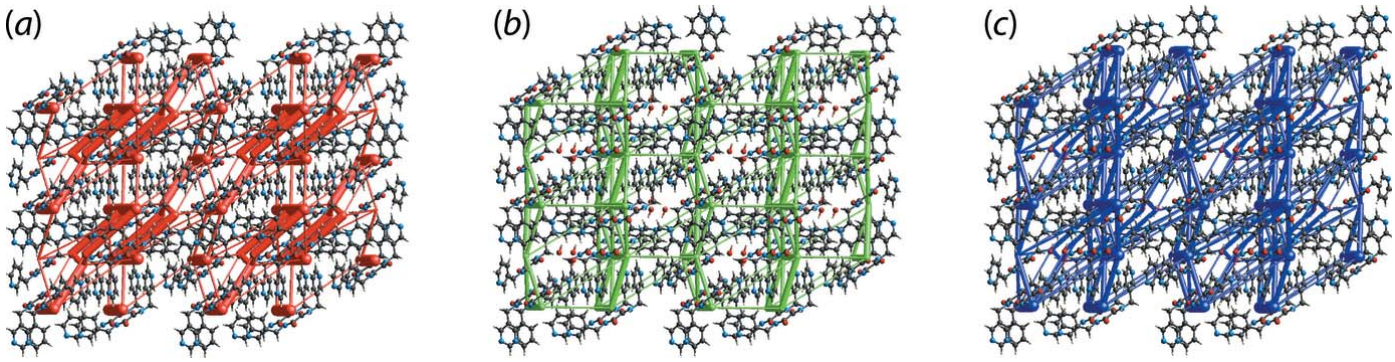

Figure 6
Perspective views of the energy framework of (I), showing the (*a*) electrostatic force, (*b*) dispersion force and (*c*) total energy diagram. The cylindrical radius is proportional to the relative strength of the corresponding energies and they were adjusted to the same scale factor of 100 with a cut-off value of 8 kJ mol^{-1} within 2 × 1 × 2 unit cells.

connected by a ten-membered $\{\cdots HNC_2O\}_2$ synthon has the greatest E_{int} energy of −73.0 kJ mol^{-1} which is comparable in energy to the classical eight-membered $\{\cdots HOCO\}_2$ synthon (Tan & Tiekink, 2019*a*). Perhaps unexpectedly, the C12–H12···C7 contact which also sustains a pair of $^3LH_2$ molecules constitutes the second strongest interaction with E_{int} = −32.7 kJ mol^{-1}, and this is followed by the C6—H6*A*···O2 (−32.0 kJ mol^{-1}), O1*W*—H1*W*···N1 (−28.6 kJ mol^{-1}), O1*W*—H2*W*···O1*W* (−26.2 kJ mol^{-1}), C7···O1 (−20.7 kJ mol^{-1}), C5—H5···N4 (−13.0 kJ mol^{-1}) and C1—H1···O1*W* (−10.5 kJ mol^{-1}) interactions. As expected, the N2—H2*N*···O1, N3—H3*N*···O2, O1*W*—H1*W*···N1 and O1*W*—H2*W*···O1*W* interactions are associated with distinct electropositive and electronegative sites and therefore, are mainly governed by electrostatic forces, while the rest of the close contacts are dispersive in nature. The relatively stable nature of the C12—H12···C7 and C6—H6*A*···O2 interactions as compared to the O1*W*—H1*W*···N1 and O1*W*—H2*W*···O1*W* interactions could be due to the presence of low repulsion energies in the former as compared to the latter.

The crystal of (I) is mainly sustained by electrostatic forces owing to the strong N2—H2*N*···O1/ N3—H3*N*···O2, O1*W*—H1*W*···N1 and O1*W*—H2*W*···O1*W* hydrogen bonding leading to a barricade-like electrostatic energy framework parallel to ($\bar{1}$01), as shown in Fig. 6(*a*). This is further stabilized by the dispersion forces arising from other supporting interactions which result in another barricade-like dispersion energy framework parallel to (100), Fig. 6(*b*). The overall energy framework for (I) is shown in Fig. 6(*c*).

Table 4
A comparison of the distribution of contacts (%) to the calculated Hirshfeld surfaces for (I) and for Forms I and II (Jotani *et al.*, 2016).

Contact	(I)	Form I	Form IIa	Form IIb
H···H	41.1	44.1	35.8	36.9
C···H/H···C	21.2	16.7	31.4	22.4
O···H/H···O	17.9	15.7	14.2	19.6
N···H/H···N	13.5	16.7	18.0	19.5
C···O/O···C	2.3	2.1	0.1	0.1
Other	3.9	4.7	0.5	1.5

A comparison of the distribution of contacts on the Hirshfeld surfaces between the $^3LH_2$ molecule in (I) and in its two polymorphic forms, *i.e.* Form I and Form II (Jotani *et al.*, 2016), with latter having two independent molecules, was performed. This analysis returned the data shown in Table 4 and indicates that $^3LH_2$ in (I) is relatively closer to Form I as compared to the independent molecules comprising Form II.

This conclusion is consistent with the analysis of the packing similarity in which a comparison of (I) and Form I exhibits an r.m.s. deviation of 0.895 Å while a comparison with Form II exhibits an r.m.s. deviation of 1.581 Å, despite only one out of 20 molecules displaying some similarity with the reference $^3LH_2$ molecule in (I), Fig. 7. The packing analysis was performed using *Mercury* (Macrae *et al.*, 2006), with the analysis criteria being set that only molecules within the 20%

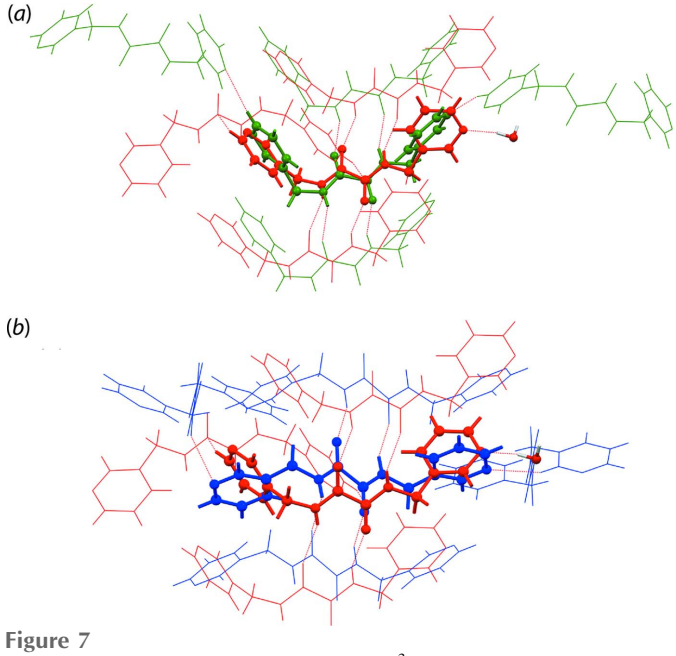

Figure 7
A comparison of the molecular packing of $^3LH_2$: (*a*) (I) (red) and Form I (green) and (*b*) (I) (red) and Form II (blue), showing the differences in terms of molecular connectivity of $^3LH_2$ with r.m.s. deviations of 0.895 and 1.581 Å, respectively.

Table 5
Geometric data, *i.e.* central C—C bond lengths (Å) and dihedral angles (°), for $^3LH_2$ in its polymorphs, solvates and (neutral) co-crystals; see Scheme 2 for the chemical diagrams of (II) and (III).

Compound	Symmetry	Conformation	C—C	$C_2N_2O_2$/(3-py)	(3-py)/(3-py)	REFCODE	Reference
Polymorphs							
Form I	–	U	1.544 (4)	74.98 (10), 84.61 (9)	88.40 (7)	OWOHAL	Jotani *et al.* (2016)
Form II[a]	$\bar{1}$	S	1.5383 (16)	77.29 (4)	0	OWOHAL01	Jotani *et al.* (2016)
	$\bar{1}$	S	1.5460 (16)	75.93 (3)	0		
Solvate							
(I)	–	U	1.541 (2)	59.71 (6), 68.42 (6)	87.86 (5)	–	This work
Co-crystals of $^3LH_2$ with							
$HO_2CCH_2N(H)C(=O)N(H)CH_2CO_2H$	$\bar{1}$	S	1.515 (3)	81.41 (7)	0	CAJQEK	Nguyen *et al.* (2001)
$HO_2CCH_2N(H)C(=O)C(=O)N(H)CH_2CO_2H$	$\bar{1}$	S	1.532 (19)	64.2 (3)	0	CAJQAG	Nguyen *et al.* (2001)
2-$NH_2C_6H_4CO_2H$	$\bar{1}$	S	1.543 (2)	74.64 (4), 74.64 (4)	0	DIDZAT	Arman *et al.* (2012)
(II)	$\bar{1}$	S	1.533 (3)	79.50 (6)	0	EMACIG	Suzuki *et al.* (2016)
$C_6F_4I_2$	$\bar{1}$	S	1.544 (4)	70.72 (9)	0	IPOSIP	Hursthouse *et al.* (2003)
2-$HO_2CC_6H_4SSC_6H_4CO_2$-2	–	U	1.543 (3)	61.22 (5), 69.43 (5)	72.12 (8)	KUZSOO	Arman *et al.* (2010)
4-$NO_2C_6H_4CO_2H$	$\bar{1}$	S	1.530 (2)	78.20 (4)	0	PAGFIP	Syed *et al.* (2016)
(III)	$\bar{1}$	S	1.550 (17)	80.5 (4)	0	REWVUM	Jin *et al.* (2013)
I—C≡C—C≡C—I	$\bar{1}$	S	1.542 (10)	76.6 (2)	0	WANNOP	Goroff *et al.* (2005)
I—C≡C—C≡C—C≡C—I	$\bar{1}$	S	1.548 (11)	84.7 (2)	0	WANPIL	Goroff *et al.* (2005)
Br—C≡C—C≡C—Br	$\bar{1}$	S	1.530 (9)	84.79 (18)	0	WUQQUW	Jin *et al.* (2015)

tolerance for both distances and angles were included in the calculation while molecules with a variation >20% were discarded, and that molecular inversions were allowed during calculation. It is therefore also apparent through this analysis that the water molecules in (I) play a crucial role in influencing the packing of $^3LH_2$ in (I).

6. Database survey

The $^3LH_2$ molecule has been characterized in two polymorphs (Jotani *et al.*, 2016) and in a number of (neutral) co-crystals. A characteristic of these structures is a long central C—C bond and conformational flexibility in terms of the relative disposition of the 3-pyridyl substituents with respect to the central $C_2N_2O_2$ chromophore (Tiekink, 2017). Indeed, the relatively long length of the central C—C bonds often attracts a level C alert in *PLATON* (Spek, 2009). Of the data included in Table 5 [for the chemical diagrams of (II) and (III), see Scheme 2], the shorter of the C—C bonds is 1.515 (3) Å, found in the co-crystal of $^3LH_2$ with $HO_2CCH_2N(H)C(=O)N(H)CH_2CO_2H$ (Nguyen *et al.*, 2001) and the longest bond of 1.550 (17) Å is found in the co-crystal of $^3LH_2$ with (III) (Jin *et al.*, 2013). In terms of conformational flexibility, the two polymorphs of $^3LH_2$ highlight this characteristic of these molecules (Jotani *et al.*, 2016). In Form I, the pyridyl rings lie to the same side of the central $C_2N_2O_2$ and therefore, have a *syn*-periplanar relationship, or, more simply, a U-shape. In Form II, comprising two independent molecules, each is disposed about a centre of inversion so the relationship is *anti*-periplanar, or S-shaped. DFT calculations revealed that the difference in energy between the two conformations is less than 1 kcal^{-1} (Jotani *et al.*, 2016). Despite this result, most of the $^3LH_2$ molecules are centrosymmetric, S-shaped. For the U-shaped molecules, the dihedral angles between the central plane and pyridyl rings range from 59.71 (6) to 84.61 (9)°. The comparable range for the S-shaped molecules, for which both dihedral angles are identical from symmetry, is 64.2 (3) to 84.79 (18)°.

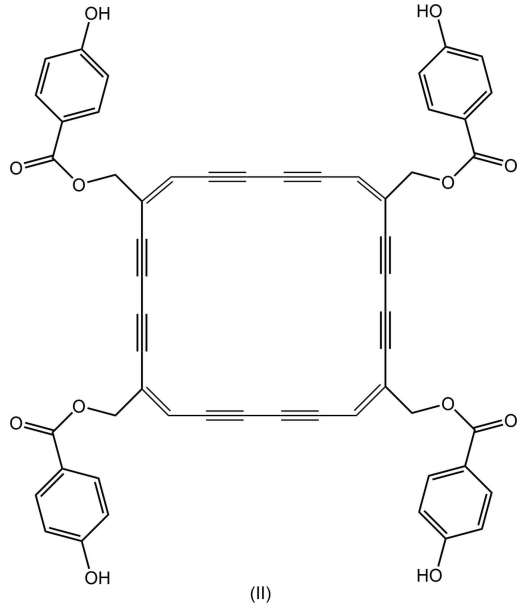

(II)

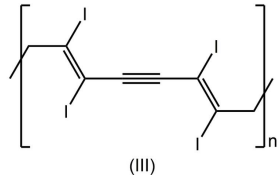

(III)

7. Synthesis and crystallization

The precursor, *N*,*N*′-bis(pyridin-3-ylmethyl)oxalamide, was prepared according to the literature (Schauer *et al.*, 1997). Crystallization of the precursor in a DMF (1 ml) and ethanol (1 ml) mixture resulted in the isolation of the title hydrate, (I); m.p.: 409.4–410.7 K. IR (cm^{-1}): 3578 ν(O—H), 3321 ν(N—H), 3141–2804 ν(C—H), 1687–1649 ν(C=O), 1524–1482 ν(C=C), 1426 ν(C—N), 710 ν(C=C).

8. Refinement

Crystal data, data collection and structure refinement details are summarized in Table 6. The carbon-bound H atoms were placed in calculated positions (C—H = 0.95–0.99 Å) and were included in the refinement in the riding-model approximation, with U_{iso}(H) set to 1.2–1.5U_{eq}(C). The oxygen- and nitrogen-bound H atoms were located in a difference-Fourier map and refined with O—H = 0.84±0.01 Å and N—H = 0.88±0.01 Å, respectively, and with U_{iso}(H) set to 1.5U_{eq}(O) or 1.2U_{eq}(N). Owing to poor agreement, one reflection, *i.e.* (551), was omitted from the final cycles of refinement.

Table 6
Experimental details.

Crystal data	
Chemical formula	$C_{14}H_{14}N_4O_2{\cdot}H_2O$
M_r	288.31
Crystal system, space group	Monoclinic, $P2_1/n$
Temperature (K)	100
a, b, c (Å)	12.4784 (4), 5.0247 (1), 22.2410 (6)
β (°)	90.170 (3)
V (Å^3)	1394.51 (6)
Z	4
Radiation type	Cu $K\alpha$
μ (mm^{-1})	0.82
Crystal size (mm)	0.09 × 0.07 × 0.03
Data collection	
Diffractometer	XtaLAB Synergy Dualflex AtlasS2
Absorption correction	Gaussian (*CrysAlis PRO*; Rigaku OD, 2018)
T_{min}, T_{max}	0.921, 1.000
No. of measured, independent and observed [$I > 2\sigma(I)$] reflections	16961, 2871, 2441
R_{int}	0.053
(sin $\theta/\lambda)_{max}$ (Å^{-1})	0.631
Refinement	
$R[F^2 > 2\sigma(F^2)]$, $wR(F^2)$, S	0.043, 0.116, 1.04
No. of reflections	2871
No. of parameters	202
H-atom treatment	H atoms treated by a mixture of independent and constrained refinement
$\Delta\rho_{max}$, $\Delta\rho_{min}$ (e Å^{-3})	0.30, −0.24

Computer programs: *CrysAlis PRO* (Rigaku OD, 2018), *SHELXS* (Sheldrick, 2015*a*), *SHELXL2017* (Sheldrick, 2015*b*), *ORTEP-3 for Windows* (Farrugia, 2012), *DIAMOND* (Brandenburg, 2006) and *publCIF* (Westrip, 2010).

Funding information

Crystallographic research at Sunway University is supported by Sunway University Sdn Bhd (grant No. STR-RCTR-RCCM-001-2019).

References

Arman, H. D., Miller, T., Poplaukhin, P. & Tiekink, E. R. T. (2010). *Acta Cryst.* E**66**, o2590–o2591.
Arman, H. D., Miller, T. & Tiekink, E. R. T. (2012). *Z. Kristallogr. Cryst. Mater.* **227**, 825–830.
Arman, H. D., Poplaukhin, P. & Tiekink, E. R. T. (2018). *Z. Kristallogr. New Cryst. Struct.* **233**, 159–161.
Brandenburg, K. (2006). *DIAMOND*. Crystal Impact GbR, Bonn, Germany.
Farrugia, L. J. (2012). *J. Appl. Cryst.* **45**, 849–854.
Goroff, N. S., Curtis, S. M., Webb, J. A., Fowler, F. W. & Lauher, J. W. (2005). *Org. Lett.* **7**, 1891–1893.
Hursthouse, M. B., Gelbrich, T. & Plater, M. J. (2003). Private communication (refcode: IPOSIP). CCDC, Cambridge, England.
Jin, H., Plonka, A. M., Parise, J. B. & Goroff, N. S. (2013). *CrystEngComm*, **15**, 3106–3110.
Jin, H., Young, C. N., Halada, G. P., Phillips, B. L. & Goroff, N. S. (2015). *Angew. Chem. Int. Ed.* **54**, 14690–14695.
Jotani, M. M., Zukerman-Schpector, J., Madureira, L. S., Poplaukhin, P., Arman, H. D., Miller, T. & Tiekink, E. R. T. (2016). *Z. Kristallogr. Cryst. Mater.* **231**, 415–425.
Macrae, C. F., Edgington, P. R., McCabe, P., Pidcock, E., Shields, G. P., Taylor, R., Towler, M. & van de Streek, J. (2006). *J. Appl. Cryst.* **39**, 453–457.
Nguyen, T. L., Fowler, F. W. & Lauher, J. W. (2001). *J. Am. Chem. Soc.* **123**, 11057–11064.
Rigaku OD (2018). *CrysAlis PRO*. Oxford Diffraction, Yarnton, England.
Schauer, C. L., Matwey, E., Fowler, F. W. & Lauher, J. W. (1997). *J. Am. Chem. Soc.* **119**, 10245–10246.
Sheldrick, G. M. (2015*a*). *Acta Cryst.* A**71**, 3–8.
Sheldrick, G. M. (2015*b*). *Acta Cryst.* C**71**, 3–8.
Spackman, M. A. & Jayatilaka, D. (2009). *CrystEngComm*, **11**, 19–32.
Spek, A. L. (2009). *Acta Cryst.* D**65**, 148–155.
Suzuki, M., Kotyk, J. F. K., Khan, S. I. & Rubin, Y. (2016). *J. Am. Chem. Soc.* **138**, 5939–5956.
Syed, S., Halim, S. N. A., Jotani, M. M. & Tiekink, E. R. T. (2016). *Acta Cryst.* E**72**, 76–82.
Tan, S. L., Halcovitch, N. R. & Tiekink, E. R. T. (2019). *Acta Cryst.* E**75**, 1133–1139.
Tan, S. L., Jotani, M. M. & Tiekink, E. R. T. (2019). *Acta Cryst.* E**75**, 308–318.
Tan, S. L. & Tiekink, E. R. T. (2019*a*). *Acta Cryst.* E**75**, 1–7.
Tan, S. L. & Tiekink, E. R. T. (2019*b*). *Z. Kristallogr. New Cryst. Struct.* **234**, 1113–1116.
Tan, S. L. & Tiekink, E. R. T. (2019*c*). *Z. Kristallogr. New Cryst. Struct.* **234**, 1117–1119.
Tan, Y. S., Chun, H. Z., Jotani, M. M. & Tiekink, E. R. T. (2019). *Z. Kristallogr. Cryst. Mater.* **234**, 165–175.
Tiekink, E. R. T. (2017). *Multi-Component Crystals: Synthesis, Concepts, Function*, edited by E. R. T. Tiekink & J. Schpector-Zukerman, pp. 289–319. Singapore: De Gruyter.
Tiekink, E. R. T. (2018). *Crystals*, **8**, article No. 18 (29 pages).
Turner, M. J., Mckinnon, J. J., Wolff, S. K., Grimwood, D. J., Spackman, P. R., Jayatilaka, D. & Spackman, M. A. (2017). *Crystal Explorer 17*. The University of Western Australia.
Westrip, S. P. (2010). *J. Appl. Cryst.* **43**, 920–925.
Wilhelm, C., Boyd, S. A., Chawda, S., Fowler, F. W., Goroff, N. S., Halada, G. P., Grey, C. P., Lauher, J. W., Luo, L., Martin, C. D., Parise, J. B., Tarabrella, C. & Webb, J. A. (2008). *J. Am. Chem. Soc.* **130**, 4415–4420.

supporting information

Acta Cryst. (2020). E**76**, 25-31 [https://doi.org/10.1107/S2056989019016153]

N,*N*′-Bis(pyridin-3-ylmethyl)ethanediamide monohydrate: crystal structure, Hirshfeld surface analysis and computational study

Sang Loon Tan and Edward R. T. Tiekink

Computing details

Data collection: *CrysAlis PRO* (Rigaku OD, 2018); cell refinement: *CrysAlis PRO* (Rigaku OD, 2018); data reduction: *CrysAlis PRO* (Rigaku OD, 2018); program(s) used to solve structure: *SHELXS* (Sheldrick, 2015*a*); program(s) used to refine structure: *SHELXL2017* (Sheldrick, 2015*b*); molecular graphics: *ORTEP-3 for Windows* (Farrugia, 2012) and *DIAMOND* (Brandenburg, 2006); software used to prepare material for publication: *publCIF* (Westrip, 2010).

N,*N*′-Bis(pyridin-3-ylmethyl)ethanediamide monohydrate

Crystal data

$C_{14}H_{14}N_4O_2{\cdot}H_2O$
M_r = 288.31
Monoclinic, $P2_1/n$
a = 12.4784 (4) Å
b = 5.0247 (1) Å
c = 22.2410 (6) Å
β = 90.170 (3)°
V = 1394.51 (6) Å^3
Z = 4
$F(000)$ = 608
D_x = 1.373 Mg m^{-3}
Cu $K\alpha$ radiation, λ = 1.54184 Å
Cell parameters from 5162 reflections
θ = 4.0–75.9°
μ = 0.82 mm^{-1}
T = 100 K
Prism, colourless
0.09 × 0.07 × 0.03 mm

Data collection

XtaLAB Synergy Dualflex AtlasS2 diffractometer
Detector resolution: 5.2558 pixels mm^{-1}
ω scans
Absorption correction: gaussian (Crysalis PRO; Rigaku OD, 2018)
T_{min} = 0.921, T_{max} = 1.000
16961 measured reflections
2871 independent reflections
2441 reflections with $I > 2\sigma(I)$
R_{int} = 0.053
θ_{max} = 76.7°, θ_{min} = 4.0°
h = −14→15
k = −6→6
l = −27→28

Refinement

Refinement on F^2
Least-squares matrix: full
$R[F^2 > 2\sigma(F^2)]$ = 0.043
$wR(F^2)$ = 0.116
S = 1.04
2871 reflections
202 parameters
0 restraints
Primary atom site location: structure-invariant direct methods
Secondary atom site location: difference Fourier map
Hydrogen site location: mixed
H atoms treated by a mixture of independent and constrained refinement
$w = 1/[\sigma^2(F_o^2) + (0.0553P)^2 + 0.7659P]$ where $P = (F_o^2 + 2F_c^2)/3$
$(\Delta/\sigma)_{max} < 0.001$
$\Delta\rho_{max}$ = 0.30 e Å^{-3}
$\Delta\rho_{min}$ = −0.24 e Å^{-3}

Special details

Geometry. All esds (except the esd in the dihedral angle between two l.s. planes) are estimated using the full covariance matrix. The cell esds are taken into account individually in the estimation of esds in distances, angles and torsion angles; correlations between esds in cell parameters are only used when they are defined by crystal symmetry. An approximate (isotropic) treatment of cell esds is used for estimating esds involving l.s. planes.

Fractional atomic coordinates and isotropic or equivalent isotropic displacement parameters (Å²)

	x	*y*	*z*	U_{iso}*/U_{eq}
O1	0.39488 (9)	−0.1106 (2)	0.53440 (5)	0.0211 (3)
O2	0.28502 (10)	0.4170 (2)	0.45056 (5)	0.0245 (3)
N1	0.51280 (11)	0.8092 (3)	0.72982 (6)	0.0230 (3)
N2	0.40224 (11)	0.3337 (3)	0.55256 (6)	0.0178 (3)
H2N	0.3890 (16)	0.486 (4)	0.5378 (9)	0.021*
N3	0.26914 (11)	−0.0297 (3)	0.43753 (6)	0.0176 (3)
H3N	0.2848 (16)	−0.182 (4)	0.4529 (8)	0.021*
N4	−0.08573 (13)	0.1419 (4)	0.36223 (9)	0.0434 (5)
C1	0.52700 (13)	0.6284 (3)	0.68624 (7)	0.0205 (3)
H1	0.598157	0.573079	0.677719	0.025*
C2	0.44417 (12)	0.5164 (3)	0.65271 (7)	0.0176 (3)
C3	0.34062 (13)	0.6008 (3)	0.66496 (7)	0.0202 (3)
H3	0.281622	0.530908	0.642955	0.024*
C4	0.32438 (13)	0.7884 (3)	0.70976 (7)	0.0224 (3)
H4	0.254145	0.849326	0.718705	0.027*
C5	0.41200 (13)	0.8860 (3)	0.74135 (7)	0.0227 (3)
H5	0.400111	1.012319	0.772402	0.027*
C6	0.47006 (13)	0.3104 (3)	0.60569 (7)	0.0202 (3)
H6A	0.545984	0.329839	0.593668	0.024*
H6B	0.461045	0.130847	0.623270	0.024*
C7	0.37291 (12)	0.1213 (3)	0.52134 (7)	0.0163 (3)
C8	0.30359 (12)	0.1859 (3)	0.46578 (7)	0.0170 (3)
C9	0.20743 (13)	−0.0186 (3)	0.38182 (7)	0.0196 (3)
H9A	0.228818	−0.169871	0.355973	0.024*
H9B	0.225732	0.147561	0.360270	0.024*
C10	0.08770 (13)	−0.0283 (3)	0.39089 (7)	0.0199 (3)
C11	0.02169 (15)	0.1432 (4)	0.35990 (9)	0.0370 (5)
H11	0.054734	0.272529	0.334924	0.044*
C12	−0.13026 (14)	−0.0379 (4)	0.39790 (8)	0.0304 (4)
H12	−0.206194	−0.042293	0.400717	0.036*
C13	−0.07261 (17)	−0.2165 (5)	0.43067 (11)	0.0486 (6)
H13	−0.107827	−0.342052	0.455703	0.058*
C14	0.03821 (16)	−0.2127 (5)	0.42700 (10)	0.0450 (6)
H14	0.079722	−0.336857	0.449325	0.054*
O1W	0.71328 (9)	0.9787 (2)	0.77119 (5)	0.0217 (3)
H1W	0.642 (2)	0.942 (4)	0.7593 (9)	0.033*
H2W	0.7244 (18)	1.141 (5)	0.7574 (10)	0.033*

Atomic displacement parameters (Å²)

	U^{11}	U^{22}	U^{33}	U^{12}	U^{13}	U^{23}
O1	0.0241 (6)	0.0137 (5)	0.0254 (6)	0.0006 (4)	−0.0029 (4)	0.0011 (4)
O2	0.0323 (7)	0.0139 (5)	0.0272 (6)	0.0018 (5)	−0.0065 (5)	0.0007 (4)
N1	0.0189 (7)	0.0242 (7)	0.0261 (7)	−0.0010 (5)	−0.0026 (5)	−0.0033 (5)
N2	0.0207 (7)	0.0122 (6)	0.0206 (6)	0.0009 (5)	−0.0012 (5)	0.0013 (5)
N3	0.0192 (7)	0.0131 (6)	0.0205 (6)	0.0005 (5)	−0.0011 (5)	−0.0001 (5)
N4	0.0187 (8)	0.0514 (11)	0.0600 (11)	0.0000 (7)	−0.0009 (7)	0.0268 (9)
C1	0.0160 (7)	0.0205 (8)	0.0248 (8)	0.0001 (6)	−0.0022 (6)	−0.0008 (6)
C2	0.0178 (7)	0.0156 (7)	0.0195 (7)	−0.0013 (6)	−0.0013 (6)	0.0023 (5)
C3	0.0161 (7)	0.0219 (8)	0.0227 (7)	−0.0035 (6)	−0.0016 (6)	0.0002 (6)
C4	0.0170 (8)	0.0263 (8)	0.0239 (7)	−0.0002 (6)	0.0023 (6)	−0.0018 (6)
C5	0.0213 (8)	0.0243 (8)	0.0226 (7)	−0.0008 (6)	−0.0003 (6)	−0.0034 (6)
C6	0.0192 (8)	0.0175 (7)	0.0239 (7)	0.0014 (6)	−0.0037 (6)	−0.0018 (6)
C7	0.0151 (7)	0.0140 (7)	0.0198 (7)	−0.0001 (5)	0.0032 (6)	0.0010 (5)
C8	0.0168 (7)	0.0151 (7)	0.0192 (7)	0.0013 (6)	0.0028 (6)	0.0003 (5)
C9	0.0195 (8)	0.0196 (7)	0.0197 (7)	−0.0003 (6)	−0.0004 (6)	−0.0012 (6)
C10	0.0206 (8)	0.0193 (7)	0.0198 (7)	−0.0013 (6)	0.0000 (6)	−0.0023 (6)
C11	0.0198 (9)	0.0432 (11)	0.0481 (11)	−0.0018 (8)	−0.0005 (8)	0.0262 (9)
C12	0.0187 (8)	0.0370 (10)	0.0355 (9)	−0.0035 (7)	0.0031 (7)	0.0028 (8)
C13	0.0268 (10)	0.0584 (14)	0.0605 (14)	−0.0057 (10)	0.0068 (9)	0.0343 (12)
C14	0.0241 (10)	0.0509 (13)	0.0601 (13)	0.0014 (9)	−0.0001 (9)	0.0345 (11)
O1W	0.0186 (6)	0.0205 (6)	0.0261 (6)	−0.0009 (5)	−0.0027 (4)	0.0012 (5)

Geometric parameters (Å, º)

O1—C7	1.2313 (18)	C4—H4	0.9500
O2—C8	1.2314 (18)	C5—H5	0.9500
N1—C5	1.341 (2)	C6—H6A	0.9900
N1—C1	1.341 (2)	C6—H6B	0.9900
N2—C7	1.3244 (19)	C7—C8	1.541 (2)
N2—C6	1.456 (2)	C9—C10	1.509 (2)
N2—H2N	0.85 (2)	C9—H9A	0.9900
N3—C8	1.323 (2)	C9—H9B	0.9900
N3—C9	1.4579 (19)	C10—C14	1.374 (2)
N3—H3N	0.86 (2)	C10—C11	1.376 (2)
N4—C12	1.326 (2)	C11—H11	0.9500
N4—C11	1.342 (2)	C12—C13	1.361 (3)
C1—C2	1.392 (2)	C12—H12	0.9500
C1—H1	0.9500	C13—C14	1.386 (3)
C2—C3	1.388 (2)	C13—H13	0.9500
C2—C6	1.507 (2)	C14—H14	0.9500
C3—C4	1.387 (2)	O1W—H1W	0.95 (2)
C3—H3	0.9500	O1W—H2W	0.88 (2)
C4—C5	1.387 (2)		
C5—N1—C1	117.34 (14)	O1—C7—N2	125.30 (14)

C7—N2—C6	121.32 (13)	O1—C7—C8	120.84 (13)
C7—N2—H2N	118.1 (13)	N2—C7—C8	113.84 (13)
C6—N2—H2N	119.8 (13)	O2—C8—N3	125.51 (14)
C8—N3—C9	122.84 (13)	O2—C8—C7	121.59 (13)
C8—N3—H3N	117.8 (13)	N3—C8—C7	112.89 (13)
C9—N3—H3N	119.4 (13)	N3—C9—C10	113.95 (12)
C12—N4—C11	116.55 (16)	N3—C9—H9A	108.8
N1—C1—C2	124.18 (15)	C10—C9—H9A	108.8
N1—C1—H1	117.9	N3—C9—H9B	108.8
C2—C1—H1	117.9	C10—C9—H9B	108.8
C3—C2—C1	117.51 (14)	H9A—C9—H9B	107.7
C3—C2—C6	123.21 (14)	C14—C10—C11	116.47 (16)
C1—C2—C6	119.28 (14)	C14—C10—C9	123.13 (15)
C2—C3—C4	119.13 (14)	C11—C10—C9	120.31 (15)
C2—C3—H3	120.4	N4—C11—C10	125.07 (17)
C4—C3—H3	120.4	N4—C11—H11	117.5
C5—C4—C3	119.17 (15)	C10—C11—H11	117.5
C5—C4—H4	120.4	N4—C12—C13	123.24 (17)
C3—C4—H4	120.4	N4—C12—H12	118.4
N1—C5—C4	122.66 (15)	C13—C12—H12	118.4
N1—C5—H5	118.7	C12—C13—C14	119.05 (18)
C4—C5—H5	118.7	C12—C13—H13	120.5
N2—C6—C2	112.50 (12)	C14—C13—H13	120.5
N2—C6—H6A	109.1	C10—C14—C13	119.61 (18)
C2—C6—H6A	109.1	C10—C14—H14	120.2
N2—C6—H6B	109.1	C13—C14—H14	120.2
C2—C6—H6B	109.1	H1W—O1W—H2W	103.3 (19)
H6A—C6—H6B	107.8		

C5—N1—C1—C2	−0.1 (2)	O1—C7—C8—O2	−176.62 (15)
N1—C1—C2—C3	0.8 (2)	N2—C7—C8—O2	4.9 (2)
N1—C1—C2—C6	−178.75 (14)	O1—C7—C8—N3	2.8 (2)
C1—C2—C3—C4	−0.5 (2)	N2—C7—C8—N3	−175.72 (13)
C6—C2—C3—C4	178.98 (14)	C8—N3—C9—C10	−94.71 (17)
C2—C3—C4—C5	−0.3 (2)	N3—C9—C10—C14	−48.5 (2)
C1—N1—C5—C4	−0.8 (2)	N3—C9—C10—C11	135.08 (17)
C3—C4—C5—N1	1.0 (3)	C12—N4—C11—C10	0.8 (3)
C7—N2—C6—C2	−146.60 (14)	C14—C10—C11—N4	−0.4 (3)
C3—C2—C6—N2	37.4 (2)	C9—C10—C11—N4	176.3 (2)
C1—C2—C6—N2	−143.09 (14)	C11—N4—C12—C13	−0.6 (3)
C6—N2—C7—O1	3.0 (2)	N4—C12—C13—C14	0.0 (4)
C6—N2—C7—C8	−178.56 (13)	C11—C10—C14—C13	−0.3 (3)
C9—N3—C8—O2	3.0 (2)	C9—C10—C14—C13	−176.9 (2)
C9—N3—C8—C7	−176.35 (12)	C12—C13—C14—C10	0.5 (4)

Hydrogen-bond geometry (Å, º)

D—H···*A*	*D*—H	H···*A*	*D*···*A*	*D*—H···*A*
N2—H2*N*···O2	0.85 (2)	2.36 (2)	2.7279 (18)	107.0 (16)
N3—H3*N*···O1	0.86 (2)	2.299 (19)	2.6924 (18)	108.0 (15)
O1*W*—H1*W*···N1	0.95 (2)	1.86 (2)	2.7958 (18)	169 (2)
O1*W*—H2*W*···O1*W*^{i}	0.88 (2)	1.97 (2)	2.8364 (15)	166 (2)
N2—H2*N*···O1^{ii}	0.85 (2)	2.03 (2)	2.8227 (18)	155.2 (18)
N3—H3*N*···O2^{iii}	0.86 (2)	2.02 (2)	2.8022 (18)	151.6 (17)
C9—H9*A*···O1*W*^{iv}	0.99	2.45	3.3772 (19)	156
C6—H6*B*···*Cg*1^{iii}	0.99	2.74	3.7043 (16)	166

Symmetry codes: (i) −*x*+3/2, *y*+1/2, −*z*+3/2; (ii) *x*, *y*+1, *z*; (iii) *x*, *y*−1, *z*; (iv) *x*−1/2, −*y*+1/2, *z*−1/2.